Available online at www.sciencedirect.com
ScienceDirect
Trans. Nonferrous Met. Soc. China 24(2014) 2346−2351
Transactions of Nonferrous Metals Society of China
www.tnmsc.cn

Microstructure and compressive deformation of hypereutectic Al−Si−Fe based P/M alloys fabricated by spark plasma sintering

Jewoosoo KIM[1], Gwang-Seon JANG[1], Mok-Soon KIM[1], Jeong-Keun LEE[2]

1. Division of Materials Science and Engineering, Inha University, Incheon, 402-751, Korea;
2. R&D Center, Dong Yang Piston Co. Ltd, Ansan, 425-120, Korea

Received 17 October 2013; accepted 12 June 2014

Abstract: Al−Si−Fe based alloys are attractive light-weight structural materials for automotive engine components because of their high wear resistance, low density and low thermal expansion. Al−17Si−5Fe−2Cu−1Mg−1Ni−1Zr alloys were produced in compact form by a spark plasma sintering (SPS) technique using gas atomized powders. The mean grain size of the compact was 530 nm, and fine equiaxed grains and uniformly distributed precipitates were observed in the compact. The compressive deformation behavior of the SPSed materials was examined at various temperatures and strain rates. All the true stress−true strain curves showed steady state flow after reaching peak stress. The peak stress decreased with increasing test temperature and decreasing strain rate. In the deformed specimens, the equiaxed grain morphology and the dislocation microstructure within the equiaxed grains were observed. These facts strongly indicated the occurrence of dynamic recrystallization during high temperature deformation of the present alloy.
Key words: Al−Si−Fe alloy; powder metallurgy; spark plasma sintering; microstructure; deformation

1 Introduction

Al−Si based alloys are used in automotive engine pistons because of their high wear resistance, low thermal expansion, and low density. In recent years, the increasing need for the development of high-performance automotive engines with a higher combustion pressure and temperature [1] has required advanced Al−Si based alloys with much higher mechanical properties at elevated temperatures. The high temperature strength of Al−Si based alloys can be improved by the addition of transition metals (TM), such as Fe [2,3]. However, a refined and uniform microstructure is difficult to obtain using a conventional ingot metallurgical process because of the limited solubility of Fe in the Al matrix and low cooling rate during solidification [4]. A powder metallurgical (P/M) route involving rapid solidification is a powerful method solving such problems. In the P/M process for Al alloys, rapidly solidified Al alloy powders are consolidated by hot pressing (HP), hot extrusion (HE), spark plasma sintering (SPS), etc. Among them the SPS technique offers unique advantages in the consolidation of Al alloy powders compared to the other consolidation techniques. SPS is a modified hot pressing process, in which an electric current is applied directly through the pressing mold and component. Rapid heating time and short process cycle can be achieved using the pulsed electric current and spark plasma effect [5−7]. Experimental and theoretical studies of the SPS process suggest the ability of SPS to produce highly dense compacts with the suppression of grain coarsening [5−11]. Such a refined and dense grain structure would be suitable for subsequent hot deformation. The hot deformed Al−Si−TM based P/M alloys using the SPSed compacts (preforms) are believed to be applicable for advanced automotive engine parts owing to the enhanced strength up to elevated temperature and good wear resistance. In this study, fully dense Al−Si−Fe based alloy compacts were produced by the SPS technique from gas atomized powders. Using the SPSed compacts, compressive deformation behavior was investigated at various temperatures and strain rates in order to provide the basic

Corresponding author: Mok-Soon KIM; E-mail: mskim@inha.ac.kr
DOI: 10.1016/S1003-6326(14)63355-0

information on the hot deformation behavior of the present alloy.

2 Experimental

Al−17Si−5Fe−2Cu−1Mg−1Ni−1Zr (mass fraction, %) powders were prepared using a gas atomization process, and the powders were consolidated to a rod type compact using SPS equipment in Korea Institute of Industrial Technology (KITECH). Most compacts were 20 mm thick with a diameter of 30 mm. Figure 1 gives an example of the external view for a compact.

Fig. 1 External view of compact

The microstructures were observed by optical microscopy and field emission-transmission electron microscopy (FE-TEM; JEOL, JEM2100F), and the porosities were analyzed using an image analyzer. The hardness was measured using a Vickers hardness tester with a 5 N load. Phase analysis was carried out by X-ray diffraction (XRD; Philips, X'Pert MPD PRO) and energy dispersive spectroscopy (EDS; Horiba, Emax 132-10). Differential thermal analysis (DTA; TA, Q600) was used to examine the thermal behavior of the compacts up to 923 K.

Compression test specimens with the dimensions of *d* 5 mm × 7.5 mm were cut from the compact. The compression test was performed at temperatures ranging from 653 to 723 K at strain rates of 1.0×10^{-3} and 3.5×10^{-1} s^{-1}. Some of the specimens deformed to approximately 20% strain were also examined by TEM. The specimens for the TEM observations were prepared using an ion milling method.

3 Results

3.1 Porosity, hardness and phase analysis of compacts

Figure 2 presents typical optical photographs without etching, showing a representative 9 parts of the cross section of the compact. As shown in this figure, the pores were barely visible. According to image analysis measurements, the porosity existed in the range of 0.2%−0.6% (see Fig. 2), indicating the successful achievement of the fully dense compact by the SPS process. The hardness values were in the range of HV 178−185 (Fig. 2).

Figure 3 shows the XRD patterns of the compact. The peaks for Al, Si, Al_5FeSi and Al_9FeSi are detected mainly in the compact consolidated by SPS. Figure 4 shows a TEM bright field image of the compact, showing fine equiaxed grains and uniformly distributed precipitates within the grains and at the grain boundaries. The mean grain size of the equiaxed grains was 530 nm. Table 1 lists the EDS analysis data for the arrows *A* (matrix) and *B* (a typical second phase) in Fig. 4. Al was detected mainly in the matrix (arrow *A*), whereas Al, Si and Fe were detected in the typical second phase (arrow *B*). The micro-chemical composition of the typical second phase corresponds to the stoichiometric composition of the Al_5FeSi phase (see Table 1). This result is in accordance with the XRD pattern in Fig. 3. Al_5FeSi was also reported to exist in a rapidly solidified Al−16Si−5Fe−0.9Cu−0.4Mg−0.9Zr alloy [2], Al−20Si−5Fe−2Ni alloy [12] and Al−10Si−5Fe−4Cu−2Mg−1Zr alloy [13].

Figure 5 presents the DTA result of the compact, in which an endothermic reaction begins from near 800 K.

3.2 Compression test

Compression tests were carried out using two different strain rates: 1.0×10^{-3} and 3.5×10^{-1} s^{-1} at temperatures between 653−723 K. Figure 6 shows the true stress−true strain curves obtained from the compression tests at various temperatures for the two strain rates. All the curves showed steady state flow after reaching the peak stress (σ_p), and the peak stress varied with test temperature and strain rate. Figure 7 shows the temperature dependence of the peak stress for different strain rates. As shown in Figs. 6 and 7, at a given strain rate, the peak stress decreased with increasing temperature, and at a given temperature, the peak stress was higher at a higher strain rate. The appearance of the peak in a flow stress curve during high temperature deformation is usually accepted as an indication for the occurrence of dynamic recrystallization. A detailed observation using TEM was made in order to find the microstructural evidence of the dynamic recrystallization, and the result will be described in the next section.

3.3 Microstructure of compressively deformed materials

Figure 8 shows the mean porosity of the specimens

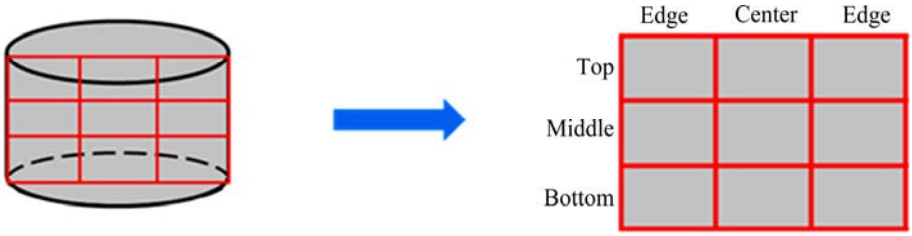

	Edge	Center	Edge
Top	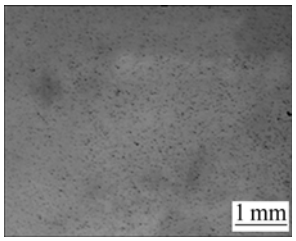 (a) Porosity: 0.6%, Hardness: HV 178	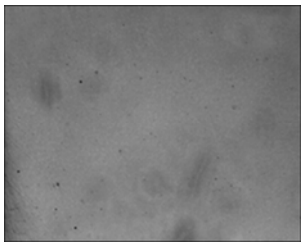 (b) Porosity: 0.2%, Hardness: HV 185	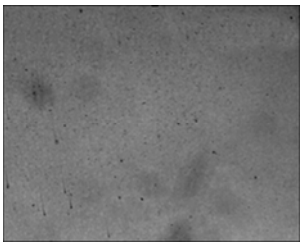 (c) Porosity: 0.5%, Hardness: HV 179
Middle	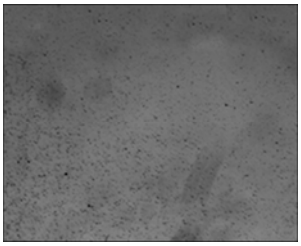 (d) Porosity: 0.4%, Hardness: HV 181	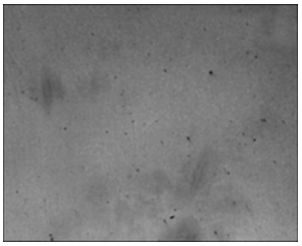 (e) Porosity: 0.2%, Hardness: HV 184	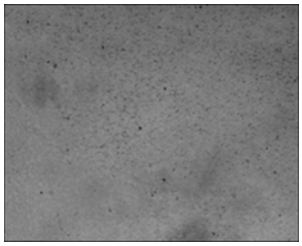 (f) Porosity: 0.4%, Hardness: HV 178
Bottom	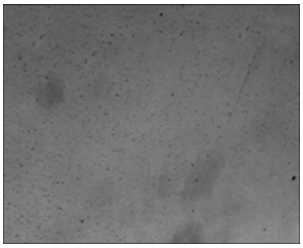 (g) Porosity: 0.2%, Hardness: HV 183	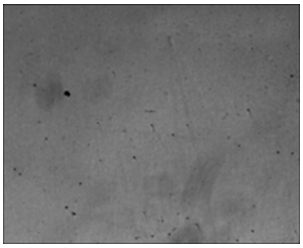 (h) Porosity: 0.3%, Hardness: HV 184	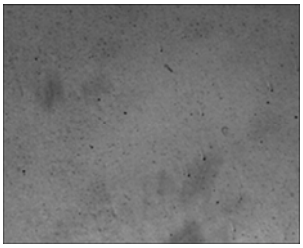 (i) Porosity: 0.2%, Hardness: HV 182

Fig. 2 OM images of cross section of compact

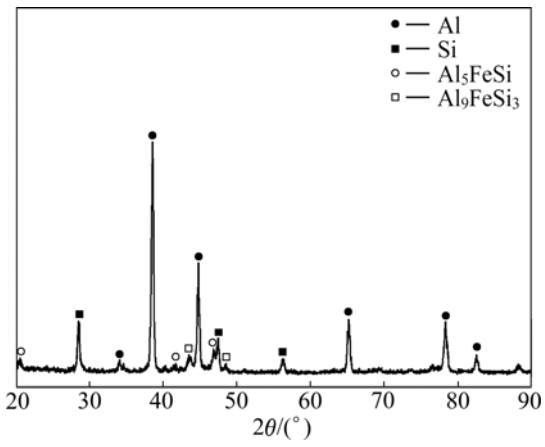

Fig. 3 XRD pattern of compact

Table 1 EDS analysis data of arrows *A* and *B* in Fig. 4

Point	Chemical composition (mole fraction)/%		
	Al	Si	Fe
A	98.89	0.82	0.29
B	73.54	15.22	11.24

after deformation. As shown in this figure, the mean porosity after deformation was less than 0.1% under all the test conditions, and lower than that of the compact (before deformation). The “Deviation” in Fig. 8 denotes the deviation of the porosity for compact.

Figure 9 shows TEM bright field images of the specimens deformed to approximately 20% compressive

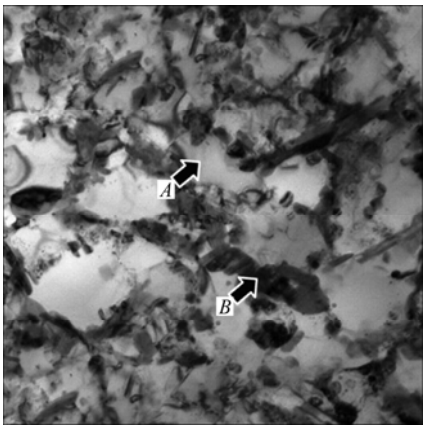

Fig. 4 TEM bright field image of compact

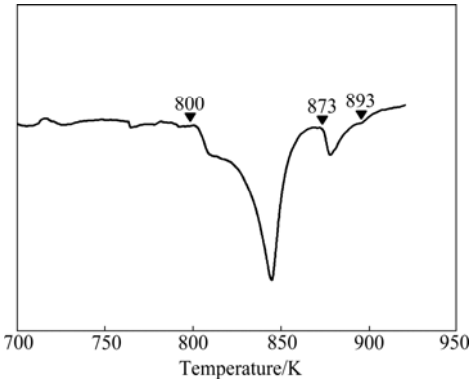

Fig. 5 DTA results for compact

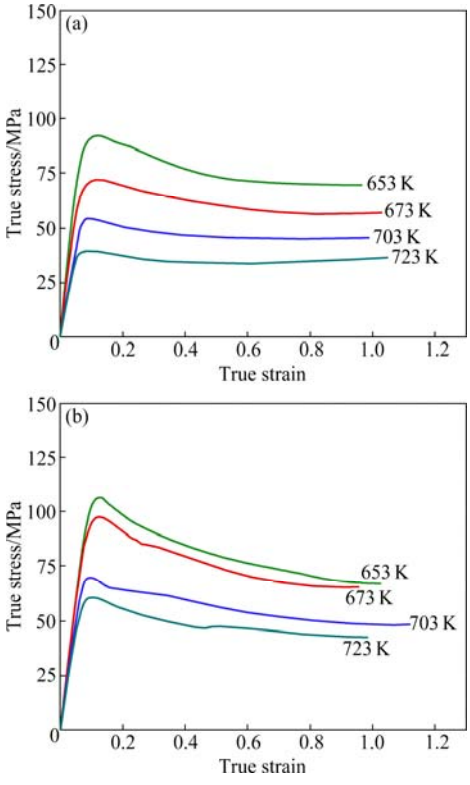

Fig. 6 True stress−true strain curves of specimens deformed at various temperatures under different strain rates: (a) 1.0×10^{-3} s^{-1}; (b) 3.5×10^{-1} s^{-1}

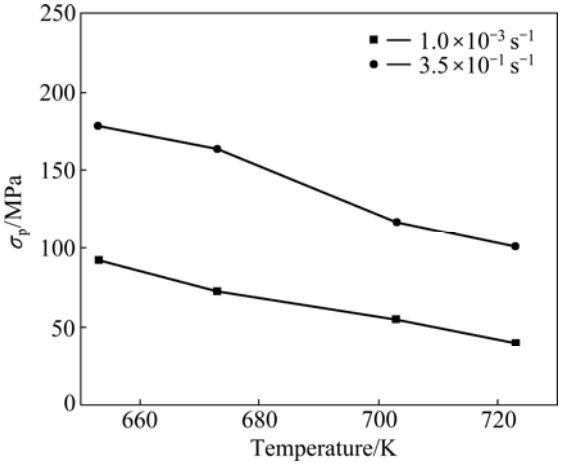

Fig. 7 Variation of peak stress with temperature at different strain rates

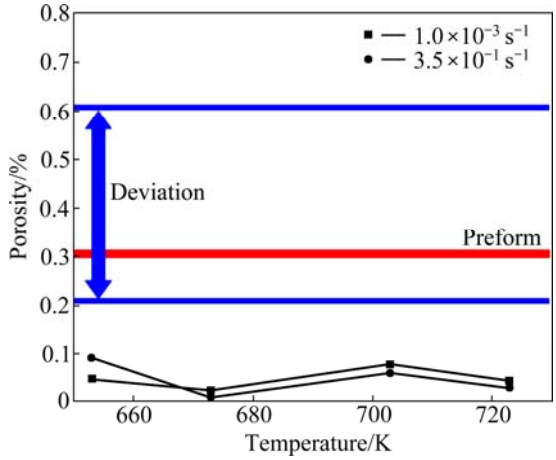

Fig. 8 Porosity of specimens deformed at various temperatures under strain rates of 1.0×10^{-3} and 3.5×10^{-1} s^{-1}

strain at a strain rate of 1.0×10^{-3} or 3.5×10^{-1} s^{-1} at 723 K. As shown in these figures, equiaxed grains were observed, and the mean grain sizes were between 860 and 920 nm. Figure 9(c) shows the dislocations within the equiaxed grains. The existence of the equiaxed grains and a number of dislocations within the equiaxed grains after plastic strain of ~20% (after reaching a peak) strongly indicate that dynamic recrystallization occurs during high temperature deformation of the present alloy. As mentioned above, the appearance of the peak stress followed by a steady state flow is another strong indication of the occurrence of dynamic recrystallization. The activation of dynamic recrystallization was also reported in a rapidly solidified Al−10Si−5Fe−1Zr alloy [11] and Al−10Si−5Fe−1Cu−0.5Mg−0.9Zr alloy [14].

4 Conclusions

1) Fine equiaxed grains and uniformly distributed fine-precipitates were observed in the compact consolidated by SPS process using rapidly solidified

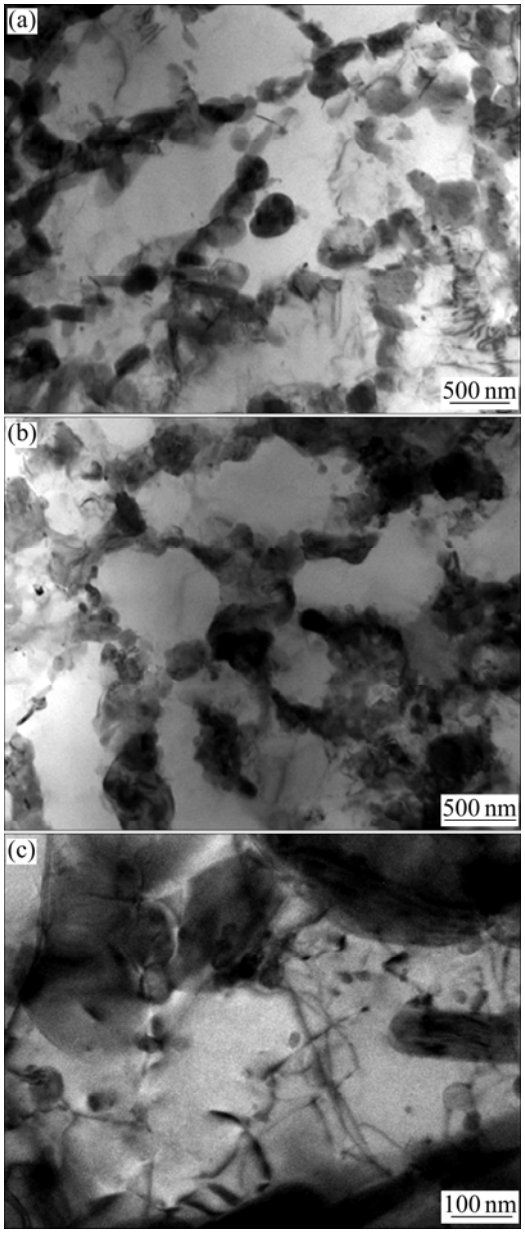

Fig. 9 TEM images of specimens deformed to 20% strain at 723 K under different strain rates: (a) 1.0×10^{-3} s^{-1}; (b), (c) 3.5×10^{-1} s^{-1}

Al−17Si−5Fe−2Cu−1Mg−1Ni−1Zr alloy powders. For the compact, the mean grain size was 530 nm, the porosity was in the range of 0.2%−0.6%, and the hardness was between HV 178−185.

2) All the true stress−true strain curves obtained by the compression tests for the compact showed a steady state flow after peak stress (σ_p). The peak stress decreased with increasing test temperature and decreasing strain rate.

3) The porosity of the deformed specimens was less than 0.1%.

4) In the deformed specimens, the equiaxed grain morphology and the dislocation microstructure within the equiaxed grains were observed. The mean grain size of the specimens deformed at 723 K under a strain rate of 1.0×10^{-3} and 3.5×10^{-1} s^{-1} was 920 and 860 nm, respectively.

5) Dynamic recrystallization was considered to occur during high temperature deformation.

Acknowledgment

The authors gratefully acknowledge the financial supports of the Ministry of Knowledge Economy (Republic of Korea) through Grant No. 10033429 and Inha University Research Grant.

References

[1] LEE J A, MUNAFO P M. High strength and wear resistant aluminum alloy for high temperature applications [R]. NASA-Marshall Space Flight Center (MSFC), 2004: 1−6.

[2] CHO H S, KIM M S. High temperature deformation behavior of Al−16Si−5Fe based alloys produced from rapidly solidified powders [J]. J Kor Inst Met & Mater, 1999, 37(10): 1191−1197.

[3] YAMAGATA H, KOIKE T. Development of P/M-aluminum-alloy piston and its world foremost mass-production [J]. J Japan Inst of Light Met, 1998, 48(1): 52−59.

[4] LIN C, WU S, ZHONG G, WAN L, AN P. Effect of ultrasonic vibration on Fe-containing intermetallic compounds of hypereutectic Al−Si alloys with high Fe content [J]. Transactions of Nonferrous Metals Society of China, 2013, 23: 1245−1252.

[5] CHEN W, ANSELMI-TAMBURINI U, GARAY J E, GROZA J R, MUNIR Z A. Fundamental investigations on the spark plasma sintering/synthesis process: I. Effect of dc pulsing on reactivity [J]. Materials Science and Engineering A, 2005, 394: 132−138.

[6] ANSELMI-TAMBURINI U, GENNARI S, GARAY J E, MUNIR Z A. Fundamental investigations on the spark plasma sintering/ synthesis process: II. Modeling of current and temperature distributions [J]. Materials Science and Engineering A, 2005, 394: 139−148.

[7] ANSELMI-TAMBURINI U, GARAY J E, MUNIR Z A. Fundamental investigations on the spark plasma sintering/synthesis process: III. Current effect on reactivity [J]. Materials Science and Engineering A, 2005, 407: 24−30.

[8] ZUNIGA A, AJDELSZTAJN L, LAVERNIA E J. Spark plasma sintering of a nanocrystalline Al−Cu−Mg−Fe−Ni−Sc alloy [J]. Metallurgical and Materials TransactionsA, 2006, 37(4): 1343−1352.

[9] YE J, AJDELSZTAJN L, SCHOENUNG J M. Bulk nanocrystalline aluminum 5083 alloy fabricated by a novel technique: Cryomilling and spark plasma sintering [J]. Metallurgical and Materials Transactions A, 2006, 37(8): 2569−2579.

[10] SASAKI T T, MUKAI T, HONO K. A high-strength bulk nanocrystalline Al−Fe alloy processed by mechanical alloying and spark plasma sintering [J]. Scripta Materialia, 2007, 57(3): 189−192.

[11] PARK S C, KIM M S, KIM K T, SHIN S Y, LEE J K, RYU K H. Compressive deformation behavior of Al−10Si−5Fe−1Zr powder alloys consolidated by spark plasma sintering process [J]. Kor J Met Mater, 2011, 49(11): 853−859.

[12] KIM T S, CHUN B S. Microstructure and mechanical property of the rapidly solidified Al−20Si−5Fe−2X (X=Ni, Cr or Zr) alloys [J]. J

Kor Inst Met & Mater, 2002, 40(8): 873−877.

[13] LEE D S, JUNG T K, KIM M S, KIM W Y, YAMAGATA H. Development of nano-structured Al−Si−Fe based bulk alloys form atomized powders [J]. Materials Science and Engineering A, 2006, 449−451: 761−764.

[14] LEE D S, SHIN, G S, KIM M S, KIM W Y, YAMAGATA H. High temperature deformation behavior of pre-sintered Al−10Si−5Fe based alloy [J]. Materials Science Forum, 2005, 475−479: 393−396.

放电等离子体烧结技术制备过共晶 Al−Si−Fe 粉末冶金合金的显微组织和压缩变形行为

Jewoosoo KIM[1], Kwang-Seon JANG[1], Mok-Soon KIM[1], Jeong-Keun LEE[2]

1. Division of Materials Science and Engineering, Inha University, Incheon, 402-751, Korea;
2. R&D Center, Dong Yang Piston Co. Ltd, Ansan, 425-120, Korea

摘　要：Al−Si−Fe 基铝合金材料由于具有高耐磨性、低密度以及低热膨胀性能，因而主要用于汽车发动机部件。利用气体雾化粉末，采用放电等离子体烧结技术制备 Al−17Si−5Fe−2Cu−1Mg−1Ni−1Zr 合金。所制备材料的晶粒尺寸为 530 nm，并且观察到细等轴晶粒和均匀分布的析出物。研究了放电等离子体烧结技术制备的材料在不同温度和应变速率下的压缩变形行为。结果表明，所有的真应力−真应变曲线在达到峰值应力后呈稳态流动趋势，随着测试温度的升高和应变速率的降低，峰值应力呈下降趋势。在变形样品中，观察到了等轴晶粒和等轴晶粒中的位错结构。这些现象说明，合金在高温变形过程中发生了动态再结晶。

关键词：Al−Si−Fe 合金；粉末冶金；放电等离子体技术；显微组织；变形

(Edited by Sai-qian YUAN)